Calculation of spin-spin zero-field splitting within periodic boundary conditions: Towards all-electron accuracy

Timur Biktagirov, Wolf Gero Schmidt, and Uwe Gerstmann

Lehrstuhl für Theoretische Materialphysik, Universität Paderborn, 33098 Paderborn, Germany

For high-spin centers, one of the key spectroscopic fingerprints is the zero-field splitting (ZFS) addressable by electron paramagnetic resonance. In this paper, an implementation of the spin-spin contribution to the ZFS tensor within the projector augmented-wave (PAW) formalism is reported. We use a single-determinant approach proposed by M. J. Rayson and P. R. Briddon [Phys. Rev. B **77**, 035119 (2008)], and complete it by adding a PAW reconstruction term which has not been taken into account before. We benchmark the PAW approach against a well-established all-electron method for a series of diatomic radicals and defects in diamond and cubic silicon carbide. While for some of the defect centers the PAW reconstruction is found to be almost negligible, in agreement with the common assumption, we show that in general it significantly improves the calculated ZFS towards the all-electron results.

I. INTRODUCTION

In recent years, spin centers in semiconducting host materials have attracted exceptional attention as promising candidates for quantum information processing [1,2] and nanoscale sensing [3,4] at ambient conditions. For many quantum applications, a spin center has to be addressed on a single-defect level. This becomes a major challenge since there are usually many other defects present in the host material, with some of them even being unidentified. Nowadays, identification and processing of spin centers relies on the combination of state-of-the-art spectroscopic techniques and first-principles simulations, whereby one can relate certain spectroscopic signatures of defects to their atomic-scale structure. For high-spin ($S \geqslant 1$) centers, one of the key spectroscopic fingerprints is the zero-field splitting (ZFS) parameter addressable by electron paramagnetic resonance (EPR) [5–8].

The ZFS describes interactions between the unpaired electrons in the absence of external magnetic field. Within perturbation theory, the ZFS can be presented as a sum of spin-spin and spin-orbit coupling contributions [9,10]. Ideally, both contributions have to be taken into account in order to achieve accurate *ab initio* predictions. However, for a number of important systems, such as spin centers in diamond and silicon carbide, the spin-spin part is believed to be dominant [6,11]. Therefore, this term alone can be of practical importance for the interpretation of the EPR spectra and identification of the spin centers.

In the last two decades, significant efforts have been made to establish the framework for ZFS calculation within all-electron density functional theory (DFT) routinely applied onto finite-size molecular systems [12,13]. This methodology is, however, not directly transferable to extended periodic systems. Even though it is sometimes possible to approximate the solid by an isolated cluster, finite-size effects may be considerable, especially for systems with strongly delocalized spin density. For point defects in semiconductors this is often the case, so the convergence with respect to cluster size can

be unreachable with reasonable computational resources. A better solution is provided by the supercell approach with explicitly imposed periodic boundary conditions, which is routinely used in computational materials science. Currently, the most effective formalism for EPR parameter calculations in extended periodic systems is based on Blöchl's projector augmented-wave (PAW) method [14]. In this method, all-electron wave functions are substituted by smooth pseudowave functions expanded in plane waves, while the true shape of the wave functions within the atomic core region are retained. This provides a way to calculate all-electron properties with the efficiency of the pseudopotential-based supercell approach. In its gauge-including extension (GIPAW) [15] which ensures the translational invariance of the wave functions in external magnetic field, this method has proved its capabilities for *ab initio* calculation of magnetic resonance parameters.

Previously, the idea to treat the ZFS tensor within the pseudopotential plane-wave framework was formulated by Rayson and Briddon [16] and revisited by Bodrog and Gali [17]. The potential capabilities of the complete PAW treatment were further addressed in the literature [11,18], but a detailed evaluation of the reconstruction scheme and a comparison with all-electron data are still missing. Even though it was possible to obtain satisfying results for some point defects by considering only smooth pseudowave functions [11], the potential significance of the on-site reconstruction of all-electron wave functions has been pointed out recently in the literature [18]. Thus, its implementation appears to be unavoidable for further applications.

Therefore, this work aims at a complete PAW-based treatment of the spin-spin ZFS. In Sec. II, we discuss the basic formulation of the spin-spin ZFS tensor within a fully reconstructed PAW formalism, where we propose an on-site reconstruction scheme, which is added in a separable way. We implement [19] these algorithms in the GIPAW module of the QUANTUM ESPRESSO package [20] and validate them (in Sec. III) against the all-electron method of the ORCA

software [21]. Benchmark calculations on various diatomic molecules and also for defects in diamond and silicon carbide (3C-SiC) demonstrate the significance of the on-site ZFS contribution for a wide range of systems.

II. THEORY

A. Spin-spin ZFS from DFT

A standard way to address the spin-spin ZFS in DFT is based on a phenomenological spin Hamiltonian, which has been thoroughly discussed in the literature related to EPR spectroscopy. Within this formalism, the first order of the perturbational ZFS Hamiltonian [22] can be parametrized in terms of a symmetric 3×3 tensor $\mathbf{D}_{\mathrm{SS}}$:

$$\hat{H}_{\mathrm{SS}} = \frac{\alpha^2}{2} \sum_{m,n} \left[\frac{\hat{\mathbf{s}}_m \hat{\mathbf{s}}_n}{r_{mn}^3} - 3 \frac{(\hat{\mathbf{s}}_m \mathbf{r}_{mn})(\hat{\mathbf{s}}_n \mathbf{r}_{mn})}{r_{mn}^5} \right] = \hat{\mathbf{S}} \mathbf{D}^{\mathrm{ss}} \hat{\mathbf{S}}. \quad (1)$$

In Eq. (1), α is the fine-structure constant, $\mathbf{r}_{mn}$ is the vector between electrons m and n, and $\hat{\mathbf{S}}$ stands for the total effective spin of the system. A conventional form for an element of the $\mathbf{D}^{\mathrm{ss}}$ tensor which separates out the spin and space parts is then given by $(a,b = x,y,z)$ [9]

$$D_{ab} = \frac{\alpha^2}{S(2S-1)} \left\langle \Psi \left| \sum_{m,n} \frac{r_{mn}^2 \delta_{ab} - 3(\mathbf{r}_{mn})_a (\mathbf{r}_{mn})_b}{r_{mn}^5} \right. \right.$$
$$\left. \left. \times \{ 2\hat{s}_{zm}\hat{s}_{zn} - \hat{s}_{xm}\hat{s}_{xn} - \hat{s}_{ym}\hat{s}_{yn} \} \right| \Psi \right\rangle, \quad (2)$$

where the sum is taken over all the orbital pairs. Note that throughout the following derivations we omit the label SS since we focus only on the spin-spin part of ZFS. The multielectron wave function Ψ in Eq. (2) is conventionally approximated by the ground-state Slater determinant. The main drawback of this approximation is that the Slater determinant constructed from spin-unrestricted DFT calculations is to a certain extent affected by spin-contamination [23]. It originates from the fact that the spin-unrestricted wave functions are no longer eigenfunctions of the total spin operator $\hat{S}^2$ but contain an artificial admixture of other spin states. In particular, this affects the spatial distribution of the orbitals and thereby introduces a certain error in the evaluated spin-spin ZFS [24]. We will come back to this point later (Sec. III C). Here, we follow the general theory of McWeeny and Mizuno [25] and write the expression for the total spin-spin ZFS as

$$D_{ab} = \sum_{m,n} f_m f_n \sigma_{mn} D_{ab,mn}, \quad (3)$$

where f_m, f_n are the occupations of orbitals m and n and σ_{mn} originates from the matrix elements of spin operators: $\sigma_{mn} = 1$ for parallel spins, and $\sigma_{mn} = -1$ in the case of antiparallel spins. In Eq. (3) the space-dependent part of the spin-spin ZFS contribution from two orbitals, m and n, is given by [25,26]

$$D_{ab,mn} = \frac{\alpha^2}{4S(2S-1)} \int d^3\mathbf{r} \, d^3\mathbf{r}'$$
$$\times \frac{|\mathbf{r} - \mathbf{r}'|^2 \delta_{ab} - 3(\mathbf{r} - \mathbf{r}')_a (\mathbf{r} - \mathbf{r}')_b}{|\mathbf{r} - \mathbf{r}'|^5}$$
$$\times [n_{mm}(\mathbf{r})n_{nn}^*(\mathbf{r}') - n_{mn}(\mathbf{r})n_{mn}^*(\mathbf{r}')], \quad (4)$$

which consists of Coulomb-like and exchangelike contributions. In the above expression we define the charge density, $n_{mn}(\mathbf{r}) = \psi_m^*(\mathbf{r})\psi_n(\mathbf{r})$, from the space distribution of the spin orbitals.

B. PAW-based formulation of spin-spin ZFS

In the following, we aim to provide a general and consistent treatment for the spin-spin ZFS given by Eq. (4) within the framework of the PAW method. This formalism relies on the transformation [14]

$$\hat{\tau} = \hat{1} + \sum_R \sum_{i \in R} [|\phi_i\rangle - |\tilde{\phi}_i\rangle]\langle \tilde{p}_i|,$$

which maps the smooth pseudowave function $\tilde{\Psi}$ expanded in plane waves back to the all-electron wave function $\Psi = \hat{\tau}\tilde{\Psi}$. Here, the index $i \in R$ refers to angular momentum quantum numbers l_i and m_i for atom R. The all-electron partial wave ϕ_i is a solution of the radial Schrödinger (or Dirac) equation for the reference atom. The pseudo-partial wave $\tilde{\phi}_i$ is equivalent to ϕ_i outside the augmentation sphere. The function $\tilde{p}_i$ is a projector localized within the core region and dual to the partial wave: $\langle \tilde{p}_i | \tilde{\phi}_j \rangle = \delta_{ij}$.

The PAW transformation allows us to reconstruct an expectation value of local operators $\langle \tilde{\Psi} | \hat{O} | \tilde{\Psi} \rangle$ in a straightforward way. In particular, this can be done for the charge density defined in Eq. (4) by noticing that $n_{mn}(\mathbf{r})$ is an expectation value of the real-space projection operator $|\mathbf{r}\rangle\langle\mathbf{r}|$. It is thus presented by a superposition

$$n_{mn}(\mathbf{r}) = \tilde{n}_{mn}(\mathbf{r}) + \sum_R \left[n_{mn}^R(\mathbf{r}) - \tilde{n}_{mn}^R(\mathbf{r}) \right] \quad (5)$$

of the smooth pseudodensity $\tilde{n}_{mn}(\mathbf{r}) = \langle \tilde{\Psi}_m | \mathbf{r} \rangle \langle \mathbf{r} | \tilde{\Psi}_n \rangle$ treated on a plane-wave grid and the difference between on-site expansions of the all-electron density n^R and the pseudodensity $\tilde{n}^R$ defined on a radial grid within the augmentation sphere around an atomic site R as

$$n_{mn}^R(\mathbf{r}) = \sum_{i,j \in R} \langle \phi_i | \mathbf{r} \rangle \langle \mathbf{r} | \phi_j \rangle \langle \tilde{\Psi}_m | \tilde{p}_i \rangle \langle \tilde{p}_j | \tilde{\Psi}_n \rangle,$$
$$\tilde{n}_{mn}^R(\mathbf{r}) = \sum_{i,j \in R} \langle \tilde{\phi}_i | \mathbf{r} \rangle \langle \mathbf{r} | \tilde{\phi}_j \rangle \langle \tilde{\Psi}_m | \tilde{p}_i \rangle \langle \tilde{p}_j | \tilde{\Psi}_n \rangle. \quad (6)$$

Similarly, we aim to construct the spin-spin ZFS in the form of three noninteracting contributions,

$$D_{ab} = \tilde{D}_{ab} + \sum_R \left[D_{ab}^R - \tilde{D}_{ab}^R \right] = \tilde{D}_{ab} + \Delta D_{ab}, \quad (7)$$

where the sum ΔD_{ab} of the on-site terms constitutes the essence of the PAW reconstruction. However, the spin-spin ZFS is an expectation value of the nonlocal two-electron operator [Eq. (1)]. For this kind of quantity, the separable form of Eq. (7) is not straightforward to obtain and requires more careful consideration [14]. It is thus illustrative to discuss the idea behind this representation by substituting the two-electron density [Eq. (5)] into the dipole-dipole interaction integral of

Eq. (7). Using the shorthand notation

$$(f|g) = \int d^3\mathbf{r}\, d^3\mathbf{r}'\, f(\mathbf{r})g^*(\mathbf{r}')$$
$$\times \frac{|\mathbf{r} - \mathbf{r}'|^2\delta_{ab} - 3(\mathbf{r} - \mathbf{r}')_a(\mathbf{r} - \mathbf{r}')_b}{|\mathbf{r} - \mathbf{r}'|^5}$$

and following Ref. [17], we write an exchange-like contribution to the ZFS as

$$(n_{mn}|n_{mn}) = (\tilde{n}_{mn}|\tilde{n}_{mn}) - 2\sum_R \left(n_{mn}^R - \tilde{n}_{mn}^R|\tilde{n}_{mn}\right)$$
$$+ \sum_R \left(n_{mn}^R - \tilde{n}_{mn}^R|n_{mn}^R - \tilde{n}_{mn}^R\right)$$
$$+ \sum_{R \neq R'} \left(n_{mn}^R - \tilde{n}_{mn}^R|n_{mn}^{R'} - \tilde{n}_{mn}^{R'}\right). \quad (8)$$

The expression for a Coulomb-like term in Eq. (4), $(n_{mm}|n_{nn})$, is entirely analogous. From Eq. (8) we can obtain the desired separable form of D_{ab} if in the first sum the plane-wave pseudodensity $\tilde{n}$ is replaced by its on-site approximation $\tilde{n}_{mn}^R$ (compare with Sec. II C of Blöchl's work [14]). This substitution is partially justified by the fact that $\tilde{n}_{mn}$ and $\tilde{n}_{mn}^R$ are exactly equal by construction within the augmentation spheres (for a complete set of projectors). However, the substitution still implies that the difference $(n_{mn}^R - \tilde{n}_{mn}^R)$ has negligible dipole-dipole interaction with the charges outside the augmentation region. With this in mind, we also leave out the last sum, which consists of intersphere contributions, and obtain the following expression [see Eq. (7)]:

$$(n_{mn}|n_{mn}) = (\tilde{n}_{mn}|\tilde{n}_{mn}) + \sum_R (n_{mn}^R|n_{mn}^R) - \sum_R (\tilde{n}_{mn}^R|\tilde{n}_{mn}^R). \quad (9)$$

In principle, very similar considerations are involved in the formulation of Hartree and exchange energies in the PAW method [14,27,28]. In this case, the problem is usually solved by introducing a so-called compensation density. The latter is constructed in such a way that upon its addition to the on-site pseudodensity, all the moments of $(n_{mn}^R - \tilde{n}_{mn}^R)$ are equal to zero individually, so that the difference produces zero electrostatic potential outside the sphere. Fortunately, we can avoid the use of the compensation in our current implementation by noticing that in the case of dipole-dipole interaction only the zeroth moment of $(n_{mn}^R - \tilde{n}_{mn}^R)$ has to vanish in order to ensure the above assumption. This can be proven by using the same analytics as in Sec. II D [in connection with Eq. (15)]. For norm-conserving pseudopotentials this requirement is always fulfilled, and this hypothesis will be further evaluated through benchmark calculations (Sec. III). Hence, we now have to provide explicit expressions and give the details of implementation for each term in Eq. (7).

C. Plane-wave pseudodensity term

The detailed analytical derivation for this term was proposed by Rayson and Briddon [16] and further revisited in Refs. [11,17,18]. Here, we mention only that it is convenient

to formulate this term in the reciprocal space as

$$\tilde{D}_{ab,mn} = \frac{\alpha^2\Omega\pi}{S(2S-1)}\sum_{\mathbf{G}}\left(\frac{G_aG_b}{G^2} - \frac{\delta_{ab}}{3}\right)$$
$$\times [\tilde{n}_{mm}(\mathbf{G})\tilde{n}_{nn}(-\mathbf{G}) - |\tilde{n}_{mn}(\mathbf{G})|^2]. \quad (10)$$

In the above expression, $\tilde{n}_{mm}(\mathbf{G})$ and $\tilde{n}_{nn}(-\mathbf{G})$ are the Fourier coefficients of the two-electron densities at points $\mathbf{G}$ and $-\mathbf{G}$, and Ω is the volume of the unit cell.

$\tilde{D}_{ab,mn}$ is the computationally most demanding term in Eq. (7). Its evaluation involves a two-step procedure. First, the pseudowave functions are Fourier transformed to the plane-wave grid in real space, where the two-electron densities are subsequently constructed. Then the densities are transferred again to the reciprocal space, and the summation in Eq. (10) is computed.

D. On-site all-electron term

We begin the analytical treatment of the on-site term by noticing that

$$\partial_a\partial_b\frac{1}{|\mathbf{r}|} = -\frac{4\pi}{3}\delta_{ab}\delta(\mathbf{r}) - \frac{|\mathbf{r}|^2\delta_{ab} - 3(\mathbf{r})_a(\mathbf{r})_b}{|\mathbf{r}|^5}. \quad (11)$$

This allows us to reformulate the integral in Eq. (4) as

$$D_{ab,mn}^R = \frac{\alpha^2}{4S(2S-1)}\int_{\Omega_R} d^3\mathbf{r}\, d^3\mathbf{r}'$$
$$\times \left[n_{mm}^R(\mathbf{r})n_{nn}^{R*}(\mathbf{r}') - n_{mn}^R(\mathbf{r})n_{mn}^{R*}(\mathbf{r}')\right]$$
$$\times \left\{\left(\frac{1}{3}\delta_{ab}\nabla^2 - \partial_a\partial_b\right)_{r'}\frac{1}{|\mathbf{r} - \mathbf{r}'|}\right\}, \quad (12)$$

where integration is restricted to the volume Ω_R of the augmentation sphere. A similar representation of the dipole-dipole interaction kernel has been previously suggested and discussed by Blöchl for evaluating the anisotropic contribution to hyperfine interaction [29]. Note that the choice of r' as a differentiation variable does not limit the generality of the following derivations, thanks to the symmetry of the kernel.

Next, we recall the definitions of the on-site densities [Eq. (6)], so that Eq. (12) can be rewritten as

$$D_{ab,mn}^R = \frac{\alpha^2}{4S(2S-1)}\sum_{i,j,k,l\,\in\,R} W_{ab,ijkl}^R$$
$$\times [\langle\tilde{\Psi}_m|\tilde{p}_i\rangle\langle\tilde{p}_j|\tilde{\Psi}_m\rangle\langle\tilde{\Psi}_n|\tilde{p}_l\rangle\langle\tilde{p}_k|\tilde{\Psi}_n\rangle$$
$$- \langle\tilde{\Psi}_m|\tilde{p}_i\rangle\langle\tilde{p}_j|\tilde{\Psi}_n\rangle\langle\tilde{\Psi}_n|\tilde{p}_l\rangle\langle\tilde{p}_k|\tilde{\Psi}_m\rangle], \quad (13)$$

where we introduce the four-partial-wave, two-electron integral,

$$W_{ab,ijkl}^R = \int_{\Omega_R} d^3\mathbf{r}\, d^3\mathbf{r}'\langle\phi_i|\mathbf{r}\rangle\langle\mathbf{r}|\phi_j\rangle\langle\phi_l|\mathbf{r}'\rangle\langle\mathbf{r}'|\phi_k\rangle$$
$$\times \left\{\left(\frac{1}{3}\delta_{ab}\nabla^2 - \partial_a\partial_b\right)_{r'}\frac{1}{|\mathbf{r} - \mathbf{r}'|}\right\}, \quad (14)$$

and account for complex conjugation. The projections of the pseudowave function $\langle\tilde{p}|\tilde{\Psi}\rangle$ in the square brackets in Eq. (13) are standard quantities in the PAW formalism. Therefore, we

can now focus on the remaining integral $W_{ab,ijkl}^R$. To simplify it, we expand the Coulomb operator in real spherical harmonics,

$$\frac{1}{|\mathbf{r} - \mathbf{r}'|} = \sum_{L,M} \frac{4\pi}{2L+1} \frac{(r_<)^L}{(r_>)^{L+1}} Y_{LM}^*(\widehat{\mathbf{r}}) Y_{LM}(\widehat{\mathbf{r}'}),$$

where $r_< = \min(r,r')$ and $r_> = \max(r,r')$. Together with the standard definition of partial waves

$$\langle \mathbf{r}|\phi_i \rangle = \frac{1}{r} u_i(r) Y_{l_i m_i}(\widehat{\mathbf{r}}),$$

this will allow us to perform the angular integration analytically and end up with numerical integration for the radial part exclusively.

During the following analysis, for each augmentation sphere we will also assume without loss of generality that the volume Ω_R is centered in the origin of the coordinates. In addition, we will further use the definition of the Clebsch-Gordan coefficients

$$C_{l_i m_i l_j m_j}^{LM} = \int d\widehat{\mathbf{r}} \, Y_{LM}^*(\widehat{\mathbf{r}}) Y_{l_i m_i}^*(\widehat{\mathbf{r}}) Y_{l_j m_j}(\widehat{\mathbf{r}})$$

and the orthonormality of spherical harmonics

$$\int d\widehat{\mathbf{r}} \, Y_{l_i m_i}^*(\widehat{\mathbf{r}}) Y_{l_j m_j}(\widehat{\mathbf{r}}) = \delta_{l_i l_j} \delta_{m_i m_j}.$$

Thereby, for the four-partial-wave, two-electron integral we obtain

$$\begin{aligned}
W_{ab,ijkl}^R = &\sum_{L,M} \frac{4\pi}{2L+1} C_{l_i m_i l_j m_j}^{LM} \int dr u_i(r) u_j(r) \\
&\times \int d\widehat{\mathbf{r}'} Y_{l_k m_k}^*(\widehat{\mathbf{r}'}) Y_{l_l m_l}(\widehat{\mathbf{r}'}) \int dr' u_k(r') u_l(r') \\
&\times \left\{ \left(\frac{1}{3}\delta_{ab}\nabla^2 - \partial_a \partial_b \right) \frac{(r_<)^L}{(r_>)^{L+1}} Y_{LM}(\widehat{\mathbf{r}'}) \right\}_{r'}. \quad (15)
\end{aligned}$$

Next, we can treat the expression in the curly brackets of Eq. (15) in a way similar to that proposed by Blöchl [29]. However, here, we have to consider separately the cases of $r > r'$ and $r < r'$.

When $r > r'$, only the terms with $L = 2$ will contribute to the magnetic dipole-dipole interaction. Now the derivative in the curly brackets,

$$\left\{ \cdots \right\}_{|L=2} = \frac{1}{r^3} \left\{ \left(\frac{1}{3}\delta_{ab}\nabla^2 - \partial_a \partial_b \right)_{r'} Y_{2M}(r') r'^2 \right\},$$

can be evaluated analytically in Cartesian coordinates for each $Y_{2M}(r')$ ($M = -2, -1, \ldots, 2$) and will be retained in the final expression as M-dependent coefficients (see Ref. [29], Eq. (A7)).

For the case of $r < r'$, the radius vector r' is in the denominator, and it is obvious that only the element with $L = 0$, $M = 0$ will contribute to D_{ab}^R. Then, it can be seen that for the expression in the curly brackets in Eq. (15) the following holds:

$$\left\{ \cdots \right\}_{|L=0} = \frac{1}{4\pi} \left(\frac{1}{3}\delta_{ab}\nabla^2 - \partial_a \partial_b \right)_{r'} \frac{1}{r'},$$

which brings us to the same line of derivations for the integral over $\mathbf{r}'$ as those followed from Eq. (14). We can notice by

exploiting Eq. (11) that Eq. (15) then becomes formally similar to the expression for the anisotropic hyperfine interaction of the density at the radius vector $\mathbf{r}'$ with the charge confined within the sphere of the radius $r < r'$. Subsequently, this leads to a form analogous to that of the $r > r'$ case and to the same set of M-dependent coefficients.

Eventually, the explicit form of the four-partial-wave, two-electron integral $W_{ab,ijkl}^R$ is easy to derive for each combination of Cartesian indexes a and b:

$$W_{xx,ijkl}^R = \sqrt{\frac{12\pi}{5}} \left(\frac{1}{\sqrt{3}} W_{3z^2-r^2}^R - W_{x^2-y^2}^R \right),$$

$$W_{yy,ijkl}^R = \sqrt{\frac{12\pi}{5}} \left(\frac{1}{\sqrt{3}} W_{3z^2-r^2}^R + W_{x^2-y^2}^R \right),$$

$$W_{zz,ijkl}^R = -\sqrt{\frac{12\pi}{5}} \sqrt{\frac{4}{3}} W_{3z^2-r^2}^R,$$

$$W_{xy,ijkl}^R = -\sqrt{\frac{12\pi}{5}} W_{xy}^R,$$

$$W_{xz,ijkl}^R = -\sqrt{\frac{12\pi}{5}} W_{xz}^R,$$

$$W_{yz,ijkl}^R = -\sqrt{\frac{12\pi}{5}} W_{yz}^R,$$

where the radial integrals are abbreviated as

$$\begin{aligned}
W_M^R = &C_{l_i m_i l_j m_j}^{2M} \delta_{k,l} \int_0^{r_c} dr \frac{u_i(r) u_j(r)}{r^3} \int_0^r dr' u_k(r') u_l(r') \\
&+ C_{l_k m_k l_j m_l}^{2M} \delta_{i,j} \delta_{k,l} \int_0^{r_c} dr u_i(r) u_j(r) \\
&\times \int_r^{r_c} dr' \frac{u_k(r') u_l(r')}{r'^3}.
\end{aligned}$$

When substituted into Eq. (13), this gives the final equation for the on-site all-electron term in spin-spin ZFS. The derivations for the on-site pseudoterm $\tilde{D}_{ab}^R$ are exactly the same, except with the pseudo-partial waves being involved instead of the all-electron ones.

III. NUMERICAL TESTS

A. Computational details

The described algorithms have been implemented in the GIPAW module of the QUANTUM ESPRESSO software. For the purpose of the following numerical exercises, we restrict ourselves to norm-conserving pseudopotentials (generated with the Troullier-Martins approach [30]) and the Perdew-Burke-Ernzerhof (PBE) exchange-correlation functional [31]. The robustness of our implementation with respect to technical parameters of the pseudopotentials (see also Ref. [18]) is illustrated in Fig. 1.

The calculations for diatomic radicals and isolated diamond and 3C-SiC clusters cut from the defect-containing supercells are carried out in a cubic supercell of 30^3 bohrs^3. Such a large supercell size has been chosen to ensure that the contribution from the spurious magnetic dipole-dipole interaction between periodic replicas is negligible. For the same reason, the Brillouin zone sampling is restricted to the Γ point. For the
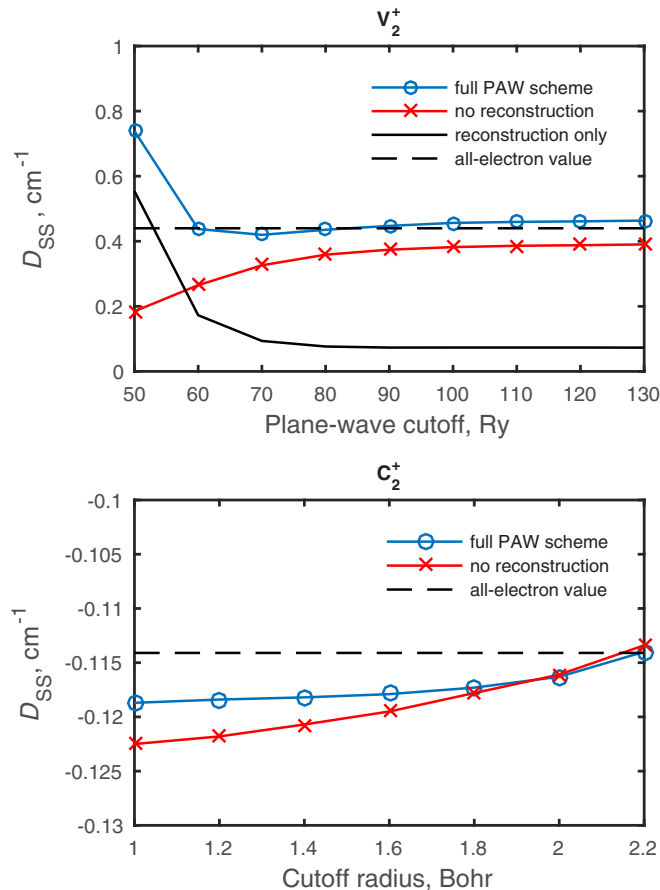
FIG. 1. Top: Convergence of the spin-spin D value for the V_2^+ radical with respect to the plane-wave cutoff. The different contributions to the D value are shown separately. Bottom: The D value of the C_2^+ radical calculated using the Troullier-Martins pseudopotential with a varying core radius.

radicals, we use a plane-wave cutoff of at least 80 Ry. In the case of main-group elements, converged results are achieved at cutoff values as low as 40 Ry, while for transition metals the convergence is slower, which is illustrated in Fig. 1 (top) for the V_2^+ radical. In the case of diamond and 3C-SiC, a cutoff of 50 Ry is already sufficient. Furthermore, for supercell calculations a k-point mesh of varying size is adopted (up to 27 k points). The defect-containing diamond and 3C-SiC supercells were optimized with the fixed lattice constants (obtained from the bulk material optimized with the PBE functional). When the experimental lattice constant was used, only minor deviations of the calculated ZFS ($<2\%$) were observed.

Note that throughout the following section we will take the notation of D and E parameters, which are commonly used in EPR spectroscopy and defined via the principle values of the **D** tensor as

$$D = D_{zz} - \tfrac{1}{2}(D_{xx} + D_{yy}), \quad E = \tfrac{1}{2}(D_{xx} - D_{yy}). \quad (16)$$

In these expressions, the coordinates are chosen so that $0 \leqslant E/D \leqslant 1/3$ and the parameter E becomes zero for axially symmetric **D** tensor.

B. High-spin diatomic radicals

For some selected systems the calculated spin-spin ZFS can be directly compared with experiment (see also Sec. III C). In general, however, the spin-orbit term (so far not included in the present implementation) prevents an unambiguous systematic evaluation of the spin-spin term against experimental data. Therefore, we validate our reconstructed PAW approach against the all-electron method implemented in the ORCA package [21]. Presently, this is the most widely used quantum-chemical code for predicting EPR parameters of molecular systems. It has been applied to a broad range of systems, thereby proving its accuracy and numerical stability, even in connection with spin-spin ZFS [12,13,23]. For evaluation of the PAW-reconstructed spin-spin ZFS, we concentrate on a series of high-spin ($S \geqslant 1$) diatomic radicals, primarily from the main group but also including examples containing third-row transition metals. The ZFS for some of these radicals was addressed by Reviakine *et al.* [32] and further revisited by Neese [12]. For the purpose of the current benchmark we focus exclusively on the spin-spin ZFS of these molecules. In order to eliminate ambiguity, we use exactly the same molecular geometries [33] and the same PBE functional for both all-electron and PAW calculations, allowing a precise comparison of the calculated spin-spin contribution.

The results are illustrated in Fig. 2 and indicate extremely good agreement of our implementation with the ORCA code. The data clearly demonstrate the significance of the on-site PAW reconstruction. Already, the bare contribution alone follows qualitatively the trend of the all-electron values. For some molecules (e.g., those containing H and C atoms exclusively) the agreement is almost perfect. But, as shown in Fig. 2(b), the reconstruction can exceed 20% of the total value for some of the radicals (seemingly upon the increase in atomic numbers). It should be noted that the relative importance of the reconstruction term is not only atom dependent. It depends also on technical details of the pseudopotential, as can be seen in Fig. 1 (bottom) for the varying cutoff radius (C_2^+ radical). Overall, the neglect of the on-site terms leads to appreciable deviation of the spin-spin ZFS from the values calculated with the all-electron approach, as illustrated graphically by a correlation plot in Fig. 2(c). As further shown by the linear regression data in Table I, the inclusion of the on-site contributions results in a clear systematic improvement despite the certain quantitative dependence of the reference data on the all-electron basis set. As clearly seen from Fig. 1 (top), the inclusion of the PAW reconstruction also gives faster convergence with respect to the energy cutoff used for the plane-wave basis set.

C. High-spin defects in diamond and *3C*-SiC

To proceed from isolated molecules to periodic systems, it appears to be natural to consider spin-triplet defect states in the diamond lattice. These kinds of paramagnetic centers are prototype examples for qubits used in spintronic applications. Thus, extensive experimental and theoretical data are available.

The first obvious choice of a test system is the negatively charged nitrogen-vacancy center (NV$^-$). At the ground state ($^3A_2$, $S = 1$) this color center manifests C_{3v} symmetry with the spin density mostly localized on the three carbon dangling bonds. Its ZFS (about 2.88 GHz in diamond [34] and 1.30 GHz
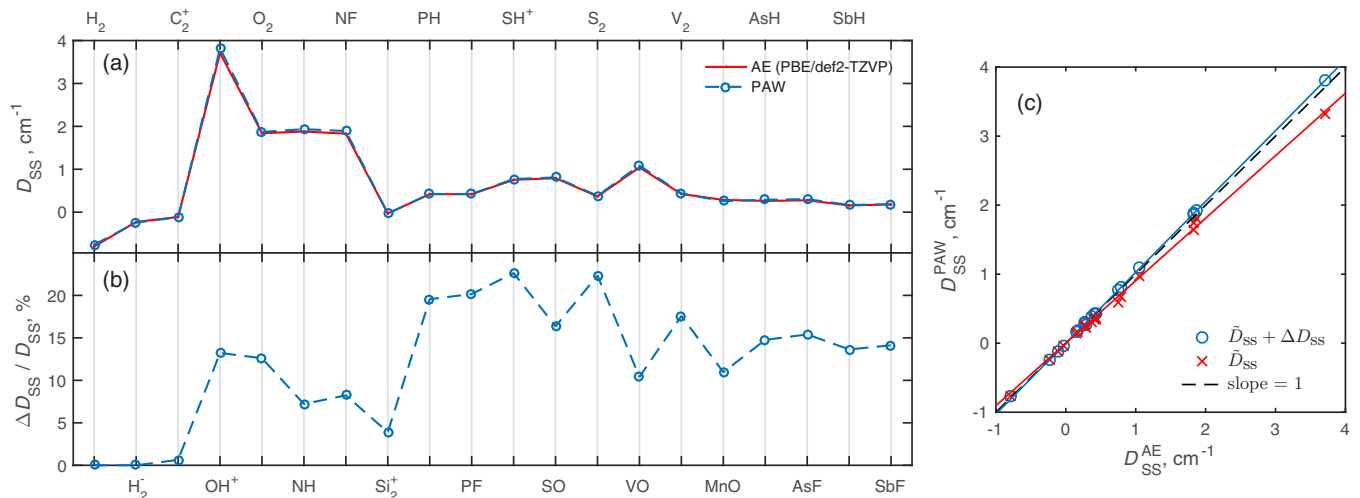
FIG. 2. (a) Spin-spin contributions to the ZFS [expressed as D values defined in Eq. (16)] for a set of diatomic radicals calculated with the PAW approach presented in this work and the all-electron (AE) method implemented in the ORCA program package. The PAW results are obtained with the PBE exchange-correlation functional, norm-conserving pseudopotentials, and a supercell size of 30^3 bohrs^3. The all-electron calculations used the PBE functional and def2-TZVP basis set of the Aldrich type. In both methods, molecular geometries taken from Ref. [33] are used if available and otherwise are relaxed using ORCA and the technical parameters described in Sec. III B. (b) Relative importance of the on-site contribution (i.e., PAW reconstruction) with respect to the total spin-spin ZFS. (c) Correlation of the all-electron and PAW results with and without the inclusion of the PAW reconstruction. For some of the considered radicals, the experimental D values can be found in Ref. [33].

in 3C-SiC [6]) is supposed to be almost entirely caused by the spin-spin contribution [11].

Aside from NV$^-$, we consider the neutral silicon-vacancy center (SiV^0) in diamond, which has attracted increasing interest throughout the last decade [35]. It has been identified as an $S = 1$ system with ZFS of about 1.00 GHz at 300 K [36] (0.94 GHz at 4 K [37]). In contrast to the NV$^-$ center, in which the impurity occupies a substitutional site neighboring the vacancy, SiV^0 adopts a split-vacancy configuration and D_{3d} symmetry with two unpaired electrons situated on the six carbon dangling bonds.

Yet another suitable test system is the neutral carbon ⟨100⟩-split interstitial (denoted below as I^0) proposed in Ref. [38] as a model for the R2 EPR center in diamond and assigned to

the EI3 center in SiC polytypes in Ref. [26]. This $S = 1$ center exhibits D_{2d} symmetry, with the spin density mostly localized on each of the two interstitial carbons. The observed ZFS is, however, axially symmetric with $D/h = \pm 4.17$ GHz and $D/h = 1.68$ GHz in diamond and SiC, respectively.

ZFS calculations have already been reported for these defect models, either with the plane-wave technique [6,11,18,39] or with the cluster approach [26,40]. However, instead of solely comparing our approach to the existing data, we also aim to validate its performance with respect to the all-electron method. Accordingly, from each of the relaxed defect-containing supercells (216 atoms) we construct a hydrogen-terminated cluster (containing 86 C atoms and 78 H atoms in the case of diamond and 43 C, 37 Si, and 78 H atoms in the case of 3C-SiC). Within the PAW supercell approach, these clusters are then immersed in a sufficiently large vacuum box (30^3 bohrs^3) to avoid spurious dipole-dipole interaction between the periodic replicas. Like for the diatomic molecules in the previous section, the geometries for PAW-based and all-electron calculations are chosen to be exactly the same.

As shown in Table II, the results manifest only minor discrepancies between the PAW and all-electron approaches. As expected from the previous tests for C-containing diatomic molecules [see the C$_2^+$ entry in Fig. 2(b)], the on-site contribution is almost entirely negligible (<1%) for NV$^-$ and SiV^0. However, it becomes surprisingly significant for I^0 (about 4% of the total value in diamond and even about 14% in 3C-SiC). This hints at why it has been possible to omit the on-site contributions for diamond in previous works [11] but shows its potential importance for the general case.

In the next step, we present the data obtained with supercell calculations and compare them with the measured values (see Table II). We use a Monkhorst-Pack [41] k-point grid up to

TABLE I. Linear regression data [the slope and the standard deviation (SD)] for the PAW-calculated spin-spin D values for a set of diatomic radicals listed in Fig. 2 in comparison with the all-electron results obtained with different basis sets, including Aldrich def2-type split valence (def2-SVP) and triple and quadruple zeta (def2-TZVP and def2-QZVP) with one polarization function. The results are listed for solely the plane-wave contribution to the ZFS as well as for the total D.

	def2-SVP	def2-TZVP	def2-QZVP[a]
Slope, $\tilde{D}_{SS}$	0.907	0.905	0.903
Slope, $\tilde{D}_{SS} + \Delta D_{SS}$	1.028	1.026	1.025
SD, $\tilde{D}_{SS}$ (%)	12.0	12.4	13.5
SD, $\tilde{D}_{SS} + \Delta D_{SS}$ (%)	4.9	3.8	4.2

[a]The all-electron results obtained with def2-QZVP for SbH and SbF radicals are found to be unreasonable and thus are not included in the linear regression analysis.

TABLE II. Spin-spin ZFS values (in cm^{-1}) for the defects in diamond and 3C-SiC described in Sec. III C. The values labeled "cluster" were obtained with the PAW approach (the smooth pseudodensity term $\tilde{D}_{SS}^{PAW}$, the on-site reconstruction term ΔD_{SS}^{PAW}, and the total value D_{SS}^{PAW}) and with the all-electron calculations in the ORCA software (D_{SS}^{AE}) for hydrogen-terminated clusters constructed from relaxed 216-atom defect-containing supercells. The label "supercell" refers to the results evaluated with the PAW approach (including the reconstruction) in 64-, 216-, and 512-atom supercells with a 50-Ry plane-wave cutoff. For the sake of completeness, the experimental values are provided in the last column.

| | Cluster | | | | Supercell | | | Experiment |
| | | | | | 64-atom | 216-atom | 512-atom | |
	$\tilde{D}_{SS}^{PAW}$	ΔD_{SS}^{PAW}	D_{SS}^{PAW}	D_{SS}^{AE}	D_{SS}^{PAW}	D_{SS}^{PAW}	D_{SS}^{PAW}	D
NV$^-$ in diamond	0.0941	0.0005	0.0946	0.0948	0.0982	0.1013	0.1028	0.0960[a]
SiV^0 in diamond	0.0280	0.0003	0.0283	0.0271	0.0303	0.0265	0.0256	0.0315[b]
I^0 in diamond	−0.1125	0.0038	−0.1088	−0.0995	−0.1123	−0.1103	−0.1100	(−)0.1390[c]
NV$^-$ in 3C-SiC	0.0594	0.0006	0.0600	0.0595	0.0553	0.0571	0.0582	0.0435[d]
I^0 in 3C-SiC	0.0677	0.0107	0.0784	0.0773	0.0770	0.0723	0.0719	0.0560[e]

[a]Reference [34].
[b]Reference [37].
[c]Reference [38].
[d]Reference [6].
[e]Reference [26].

(3 × 3 × 3) for supercells containing 64, 216, and 512 atoms. The observed deviations with respect to the varying supercell size can originate directly from the dipole-dipole interaction between the periodic replicas and indirectly from the strain-induced redistribution of the spin density within the supercell. In either case, the results for larger supercells are expected to be more reliable despite the somewhat better agreement with experiment found for the smaller ones.

As the bottom line, independent of the convergence behavior of the supercell calculations, the agreement between the reconstructed PAW approach and the all-electron method observed for the cluster calculations suggests that the spin-spin ZFS is reliably described in our implementation. Then it can be argued that besides the influence of the exchange-correlation functional used in the DFT calculation [12], the discrepancies between the measured D values and our supercell calculations can be at least partially due to the absence of the spin-orbit contribution. The hypothesis of the second-order effect already being significant for defects in diamond was recently addressed in Ref. [40]. It thus motivates future efforts to extend the PAW-based framework to spin-orbit ZFS.

A further possible source for deviation from the experiment is given by the mentioned spin contamination. Due to the construction of the D expectation values from ground-state Slater determinants (see Sec. II), an overestimated partial antiferromagnetic coupling in paramagnetic states also affects the calculated spin-spin ZFS. In all-electron methods, the spin contamination is often corrected by constructing the ground-state wave function of the system [see Eq. (2)] from (i) open-shell spin-restricted orbitals or (ii) spin-unrestricted natural orbitals. While being clean of spin contamination, the open-shell spin-restricted treatment does not preserve physically relevant spin polarization, whereas the performance of the second approach is believed to rely to a certain extent on error cancellation [23]. There is also no evidence that this will, in general, improve the accuracy of the ZFS calculation for spin centers in semiconductors, where due to the presence of valence bands the effect of spin contamination is less

prominent and where the concept of the natural orbitals is less straightforward. A final unambiguous conclusion, however, will again be possible only upon implementation of the spin-orbit contribution and by comparing the full ZFS tensor with experiment.

IV. SUMMARY

To summarize, we have proposed a complete formulation for spin-spin ZFS within the formalism of the PAW method [14]. We revisited the existing approach for the smooth pseudodensity part and further provided the solution for the on-site reconstruction which has not been investigated explicitly in previous works. The proposed algorithms were then implemented into a plane-wave pseudopotential code and validated against the all-electron approach of the ORCA program package. The results exhibit extremely small discrepancies showing that the approximations underlying the proposed separation of the plane-wave and on-site terms [Eq. (8)] are justified.

It is important to emphasize that we have observed an almost negligible effect of the on-site reconstruction for some of the defect centers in the diamond lattice. Historically, diamond was the first test system for the plane-wave-based calculation of the spin-spin ZFS [16,17]. The satisfying results obtained in those works with solely the smooth pseudodensity contribution have led to an impression that the on-site terms can be ignored with no loss of accuracy. However, by means of benchmark calculations on diatomic molecules we clearly illustrate that this is not true in general. The results suggest that the effect of on-site reconstruction is strongly atom specific. It is seemingly more pronounced for heavier elements, but a general trend or even an empirical rule cannot be found. The inclusion of the on-site terms reduces the influence of the technical details of the pseudopotentials and improves the convergence with respect to k-point sampling and energy cutoff. It thus leads to a systematic correction of the plane-wave results towards the all-electron values.

In this way, the presented PAW approach provides a general treatment for the spin-spin ZFS of periodic systems. Its benefit is, of course, not limited to systems where the spin-spin part is the dominating one. It will be necessary even for paramagnetic centers which are not yet fully addressable due to the missing spin-orbit term (e.g., transition-metal ions).

[1] D. DiVincenzo, Nat. Mater. **9**, 468 (2010).

[2] D. D. Awschalom, L. C. Bassett, A. S. Dzurak, E. L. Hu, and J. R. Petta, Science **339**, 1174 (2013).

[3] H. J. Mamin, M. Kim, M. H. Sherwood, C. T. Rettner, K. Ohno, D. D. Awschalom, and D. Rugar, Science **339**, 557 (2013).

[4] P. Maletinsky, S. Hong, M. S. Grinolds, B. Hausmann, M. D. Lukin, R. L. Walsworth, M. Loncar, and A. Yacoby, Nat. Nanotechnol. **7**, 320 (2012).

[5] V. A. Soltamov, B. V. Yavkin, D. O. Tolmachev, R. A. Babunts, A. G. Badalyan, V. Yu. Davydov, E. N. Mokhov, I. I. Proskuryakov, S. B. Orlinskii, and P. G. Baranov, Phys. Rev. Lett. **115**, 247602 (2015).

[6] H. J. von Bardeleben, J. L. Cantin, A. Csóré, A. Gali, E. Rauls, and U. Gerstmann, Phys. Rev. B **94**, 121202(R) (2016).

[7] H. J. von Bardeleben, J. L. Cantin, E. Rauls, and U. Gerstmann, Phys. Rev. B **92**, 064104 (2015).

[8] A. Csóré, H. J. von Bardeleben, J. L. Cantin, and A. Gali, Phys. Rev. B **96**, 085204 (2017).

[9] J. E. Harriman, *Theoretical Foundations of Electron Spin Resonance* (Academic, New York, 1978).

[10] F. Neese, in *The Quantum Chemical Calculation of NMR and EPR Properties* (Wiley-VCH, Heidelberg, 2004), p. 541.

[11] V. Ivády, T. Simon, J. R. Maze, I. A. Abrikosov, and A. Gali, Phys. Rev. B **90**, 235205 (2014).

[12] F. Neese, J. Chem. Phys. **127**, 164112 (2007).

[13] F. Neese, J. Am. Chem. Soc. **128**, 10213 (2006).

[14] P. E. Blöchl, Phys. Rev. B **50**, 17953 (1994).

[15] C. J. Pickard and F. Mauri, Phys. Rev. B **63**, 245101 (2001).

[16] M. J. Rayson and P. R. Briddon, Phys. Rev. B **77**, 035119 (2008).

[17] Z. Bodrog and A. Gali, J. Phys. Condens. Matter **26**, 015305 (2013).

[18] H. Seo, H. Ma, M. Govoni, and G. Galli, Phys. Rev. Mater. **1**, 075002 (2017).

[19] P. Giannozzi, O. Andreussi, T. Brumme, O. Bunau, M. Buongiorno Nardelli, M. Calandra, R. Car, C. Cavazzoni, D. Ceresoli, M. Cococcioni, N. Colonna, I. Carnimeo, A. Dal Corso, S. de Gironcoli, P. Delugas, R. A. DiStasio, Jr., A. Ferretti, A. Floris, G. Fratesi, G. Fugallo, R. Gebauer, U. Gerstmann, F. Giustino, T. Gorni, J. Jia, M. Kawamura, H.-Y. Ko, A. Kokalj, E. Kkbenli, M. Lazzeri, M. Marsili, N. Marzari, F. Mauri, N. L. Nguyen, H.-V. Nguyen, A. Otero-de-la-Roza, L. Paulatto, S. Poncé, D. Rocca, R. Sabatini, B. Santra, M. Schlipf, A. P. Seitsonen, A. Smogunov, I. Timrov, T. Thonhauser, P. Umari, N. Vast, X. Wu, and S. Baroni, J. Phys. Condens. Matter **29**, 465901 (2017).

[20] P. Giannozzi, S. Baroni, N. Bonini, M. Calandra *et al.*, J. Phys. Condens. Matter **21**, 395502 (2009).

[21] F. Neese, Wiley Interdiscip. Rev. Comput. Mol. Sci. **2**, 73 (2012).

[22] R. McWeeny, *Methods of Molecular Quantum Mechanics* (Academic Press, London, 1992).

[23] S. Sinnecker and F. Neese, J. Phys. Chem. A **110**, 12267 (2006).

[24] The sensitivity of the spin-unrestricted ZFS to spin contamination arises from its sum-over-orbital pairs formulation. If the spatial distribution of each orbital deviates for the two spin channels, the individual cross-spin terms can add up to sometimes completely unrealistic values. From a technical standpoint, this forces us to further include (otherwise unphysical) $m = n$ cross terms in the sum over pairs in order to get a numerically robust implementation.

[25] R. McWeeny and Y. Mizuno, Proc. R. Soc. Lond. A **259**, 554 (1961).

[26] T. T. Petrenko, T. L. Petrenko, and V. Ya Bratus, J. Phys. Condens. Matter **14**, 12433 (2002).

[27] G. Kresse and D. Joubert, Phys. Rev. B **59**, 1758 (1999).

[28] J. Paier, R. Hirschl, M. Marsman, and G. Kresse, J. Chem. Phys. **122**, 234102 (2005).

[29] P. E. Blöchl, Phys. Rev. B **62**, 6158 (2000).

[30] N. Troullier and J. L. Martins, Phys. Rev. B **43**, 1993 (1991).

[31] J. P. Perdew, K. Burke, and M. Ernzerhof, Phys. Rev. Lett. **77**, 3865 (1996).

[32] R. Reviakine, A. V. Arbuznikov, J.-C. Tremblay, C. Remenyi, O. L. Malkina, V. G. Malkin, and M. Kaupp, J. Chem. Phys. **125**, 054110 (2006).

[33] K. P. Huber and G. Herzberg, *Constants of Diatomic Molecules, Molecular Spectra and Molecular Structure* (Van Nostrand Reinhold, New York, 1979).

[34] J. Loubser and J. van Wyk, Rep. Prog. Phys. **41**, 1201 (1978).

[35] U. F. S. D'Haenens-Johansson, A. M. Edmonds, B. L. Green, M. E. Newton, G. Davies, P. M. Martineau, R. U. A. Khan, and D. J. Twitchen, Phys. Rev. B **84**, 245208 (2011).

[36] A. M. Edmonds, M. E. Newton, P. M. Martineau, D. J. Twitchen, and S. D. Williams, Phys. Rev. B **77**, 245205 (2008).

[37] B. C. Rose, G. Thiering, A. M. Tyryshkin, A. M. Edmonds, M. L. Markham, A. Gali, S. A. Lyon, and N. P. de Leon, arXiv:1710.03196.

[38] D. C. Hunt, D. J. Twitchen, M. E. Newton, J. M. Baker, T. R. Anthony, W. F. Banholzer, and S. S. Vagarali, Phys. Rev. B **61**, 3863 (2000).

[39] M. J. Rayson, J. P. Goss, and P. R. Briddon, Phys. B (Amsterdam, Neth.) **340**, 673 (2003).

[40] A. Komarovskikh, A. Dmitriev, V. Nadolinny, and Y. Palyanov, Diamond Relat. Mater. **76**, 86 (2017).

[41] H. J. Monkhorst and J. D. Pack, Phys. Rev. B **13**, 5188 (1976).